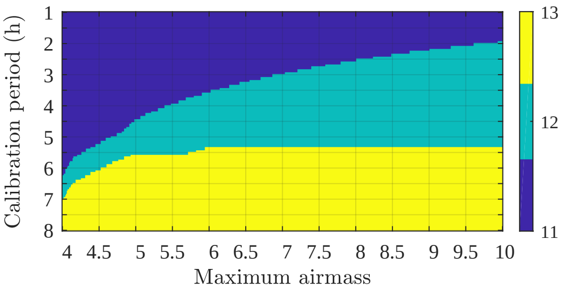

Figure A2. Number of available catalogue stars for a multi-star calibration, during a 24 h period. The following constraints were employed in generating the tri-color contours: at least one star at $x < 1.2$, exclusion of any star of visual magnitude $V > 1.5$ for $x > 6$, as well as $V > 2$ at $x > 5$.

A calibration can, for example, be carried out in 2 h with only 11 stars of our 13 star dataset (Figure 3). A 12 star calibration can be carried out only if $x < 9.5$, or if the calibration period is > 2.5 h.

Appendix B: Relative importance of component errors

From equation (7) and (8) one gets the error propagation into the τ Langley retrieval

$$\sigma^2_{\hat{\tau}} = \frac{\sigma^2_{\overline{\tau}}}{\sigma^2_x} = \frac{1}{\sigma^2_x}\left(\sigma^2_{\overline{\epsilon}_S} + \overline{x^2}\sigma^2_{\overline{\tau}} + \sigma^2_{\overline{\epsilon}_{M_0}}\right) \tag{B1}$$

$$\sigma^2_{\hat{\tau}} = k_1\sigma^2_{\overline{\epsilon}_S} + k_2\sigma^2_{\overline{\tau}} + k_1\sigma^2_{\overline{\epsilon}_{M_0}}, \text{with } k_1 = \frac{1}{\sigma^2_x}, k_2 = \frac{\overline{x^2}}{\sigma^2_x} \tag{B2}$$

Error propagation into the calibration constant (C) retrieval is, in a similar fashion, expressed as

$$\sigma^2_{\hat{C}} = \sigma^2_{\hat{\tau}}\overline{x^2} = \frac{\overline{x^2}}{\sigma^2_x}\left(\sigma^2_{\overline{\epsilon}_S} + \overline{x^2}\sigma^2_{\overline{\tau}} + \sigma^2_{\overline{\epsilon}_{M_0}}\right) \tag{B3}$$

$$\sigma^2_{\hat{C}} = k_2\sigma^2_{\overline{\epsilon}_S} + k_3\sigma^2_{\overline{\tau}} + k_2\sigma^2_{\overline{\epsilon}_{M_0}}, \text{with } k_3 = \frac{\overline{x^2}^2}{\sigma^2_x} \tag{B4}$$

The coefficients k_1, k_2 and k_3 are displayed in Figure B1b, c and d, respectively, for the x protocols of Figure B1a. The blue curve shows uniformly distributed values of x, while the red curve shows a more realistic observing configuration of constant time intervals[13]. In order to investigate more practical (smaller) ranges, the working range is incrementally truncated from both, the right and left (the solid and dashed curves, respectively). ~~The focus is on two particular ranges: $x < 5$ (red-filled circles)~~A particular focus is placed on two x-ranges: the solid red circles for which $x < 5$, where $k_1 \simeq 1.2$, $k_2 \simeq 5.3$ and $k_3 \simeq 23$ (~~approximately-stabilized for $X \gtrsim 4$~~the k_3 red curve flattens out for $X > 5$ in Figure B1d), and ~~$x > 5$ (~~the open red circles ~~)~~for which $x > 5$, where $k_1 \simeq 0.5$, $k_2 \simeq 25$ and $k_3 \simeq 1250$ (~~i.e. >~~ k_3 being 50 times ~~greater than that for~~ the "$x < 5$" value). This strong~~weighting towards large~~, large-x weighting drives the standard error in C. ~~The term $\sigma_{\overline{\epsilon}_S}$ is typically $\sim \sigma_{\overline{\tau}}$, which is, in~~

[13] Both conditions apply to a star crossing the meridian at zenith.

turn $\sim \sigma_{\epsilon_{M_0}}$ Ivănescu et al. (2021). The $\sigma^2_{\hat{\tau}}$ term may, accordingly, tend to dominate the $\overline{\epsilon_S}^2$ and $\sigma^2_{\bar{\epsilon}_{M_0}}$ terms in $\sigma_{\epsilon_{S_z}}$ (the zenith value of σ_{ϵ_S}) is typically $\sim \sigma_\tau$, and thus $\sim \sigma_{\epsilon_{M_0}}$ (Ivănescu et al., 2021). Since ϵ_S depends on x[14], $k_2\sigma^2_{\bar{\epsilon}_S} \simeq k_3\sigma^2_{\bar{\epsilon}_{S_z}}$[15]$\sim k_3\sigma^2_{\bar{\tau}}$, both first terms of equation (B3)[16] B4) being driven by k_3, which flattens out for $x \in [1.086, X]$, with $X > 5$. They will generally tend then to dominate $k_2\sigma^2_{\bar{\epsilon}_{M_0}}$ (unless $N \ll n$), and thus the $\sigma_{\hat{C}}$ calibration error, particularly for large x-ranges.

Appendix C: Error discussion supplement

The C values, derived from tangents applied to the Figure 8 solid curves (the means of a $\Delta x = 1.5$ sliding window), are plotted in Figure C1. The objective of this plot is to highlight more robust (lower frequency) C variations (and thus C errors) as a function of x. The 400 nm C values are relatively stable up to $x \simeq 7$ to 7.5 where they are subject to a large increase. The 1000 nm C pattern is similar with an increase beginning at $\simeq 9$ (observations that are roughly consistent with the vignetting arguments of subsection 6.2).

Author contributions. Liviu Ivănescu: conceptualization, methodology, data curation, software, formal analysis, investigation, writing original draft. Norman T. O'Neill: validation, writing, review and editing, supervision, funding acquisition.

Competing interests. No competing interests are present.

Acknowledgements. This work was supported by CANDAC (the Canadian Network for the Detection of Atmospheric Change) via the NSERC PAHA (Probing the Atmosphere of the High Arctic) project, by the NSERC CREATE Training Program in Arctic Atmospheric Science, as well as by the grant 21SUASACOA and the FAST program of the Canadian Space Agency (CSA). Finally we also gratefully acknowledge the support of the CANDAC operations staff at Eureka for their numerous troubleshooting interventions.

[14] See for example the ϵ_S increase with x in Figure 8.

[15] If we assume $\epsilon_S \simeq \epsilon_{S_z} x$, for a multi-star calibration with $n = n_i N$ (see details in section 3.2, footnote 3), $\sigma^2_{\bar{\epsilon}_S} = (\sum_{i=1}^{n} \epsilon^2_{S_i})/n \simeq (\sum_{j=1}^{n_i} \epsilon^2_{S_{z,j}} \sum_{k=1}^{N} x_k^2)/(n_i N) = \sigma^2_{\bar{\epsilon}_{S_z}} \overline{x^2}$.

[16] Since, as per Figure B1e, $4 < x^2 < 50$.